

To appear in *Molecular Simulation*
 Vol. 00, No. 00, Month 20XX, 1–15

arXiv:1509.02227v2 [cond-mat.stat-mech] 4 Nov 2015

Disordered vortex matter out of equilibrium: a Langevin molecular dynamics study

Hiba Assi^a, Harshwardhan Chaturvedi^a, Ulrich Dobramysl^b, Michel Pleimling^{a,c} * and Uwe C. Täuber^a

^a*Department of Physics (MC 0435), 850 West Campus Drive, Virginia Tech, Blacksburg, VA 24061, USA;*

^b*Mathematical Institute, University of Oxford, Andrew Wiles Building, Radcliffe Observatory Quarter, Woodstock Road, Oxford OX2 6GG, UK;* ^c*Academy of Integrated Science (MC 0405), 300 Turner Street NW, Virginia Tech, Blacksburg, VA 24061, USA*

(Received 00 Month 20XX; final version received 00 Month 20XX)

We discuss the use of Langevin molecular dynamics in the investigation of the non-equilibrium properties of disordered vortex matter. Our special focus is set on values of system parameters that are realistic for disordered high- T_c superconductors such as YBCO. Using a discretized elastic line model, we study different aspects of vortices far from thermal equilibrium. On the one hand we investigate steady-state properties of driven magnetic flux lines in a disordered environment, namely the current-voltage characteristics, the gyration radius, and the pinning time statistics. On the other hand we study the complex relaxation processes and glassy-like dynamics that emerge in type-II superconductors due to the intricate competition between the long-range vortex-vortex repulsion and flux pinning due to randomly placed point defects. To this end we consider different types of sudden perturbations: temperature, magnetic field, and external current quenches.

Keywords: Langevin molecular dynamics; disordered vortex matter; type-II superconductors; pinning statistics; relaxation processes

1. Introduction

Langevin equations are stochastic differential equations that have seen widespread applications in many areas of physics [1]. They form a sound effective description in situations where a strict separation of time scales prevails, i.e., where one has both fast and slow degrees of freedom. Langevin equations then provide equations of motion for the relevant slow modes, whereas the effects of the fast degrees (e.g., the environment) are incorporated via stochastic forcing.

Since the initial use of a Langevin equation for the description of a Brownian particle [2], many other problems have been tackled using stochastic differential equations. Obvious problems can be found in biological settings where large 'particles' are moving in an aqueous environment. But there are also important problems in condensed matter and material physics that can be successfully addressed using Langevin equations. Well-known examples include domain walls in magnetic systems, fluctuating interfaces, or flux lines in type-II superconductors.

In this paper we discuss the use of Langevin equations for the study of interacting vortices in a disordered environment. Our main focus is on high- T_c superconductors [3] where glassy states are realized at low temperatures due to the competition of long-range vortex-vortex interaction and short-range defect pinning. More specifically, we will discuss in some detail the properties of these systems when they are forced far away from thermal equilibrium. By employing the methods of Langevin molecular dynamics, we numerically solve the set of coupled stochastic differential equa-

*Corresponding author. Email: pleim@vt.edu

tions describing our systems. In particular, our model systems are well suited for the application of this method due to the separation into many slow degrees of freedom embedded in an environment dominated by fast fluctuating thermal degrees of freedom.

In principle, a system can be prepared 'far from equilibrium' in two different ways. In the first case the system is subjected to an external drive that yields a non-equilibrium steady state. Non-equilibrium steady states have been a focus of many studies in statistical physics that aim at finding a comprehensive theoretical framework allowing to determine the stationary probability density and probability current distribution. Whereas some progress has been made in certain instances, a comprehensive theory remains elusive. Non-equilibrium steady states are also of interest in the context of vortex matter as they emerge naturally when applying a driving force to the system.

Another way to induce a system out of equilibrium is to force it away from a stationary state through a sudden change of at least one of the system parameters [4]. This sudden change, often called quench, can be realized in different ways. Very common is a temperature quench, but other types of quenches (magnetic field or vortex density as well as external current or drive quenches) are also possible and will be discussed in this paper. Once the system has been brought out of the initial steady state, it will relax towards a new stationary state. This relaxation process can be very long-lasting in systems with slow or glassy-like dynamics. In some instances this relaxation process manifests itself through characteristic dynamical scaling behavior [5]. In other cases relaxation is a very involved process, due to the competition between different physical interactions or other effects, and time-dependent quantities may exhibit a very rich and complex behavior. The intricate slow relaxation processes of interacting magnetic vortices in disordered type-II superconductors deep inside the low-temperature Bragg glass phase are of this second type.

This paper is meant to provide a didactic introduction to the investigation of non-equilibrium properties of flux lines in a disordered environment using Langevin molecular dynamics. After introducing the basics of Langevin dynamics in the next section, we focus in section 3 on the study of interacting vortex matter using Langevin molecular dynamics. We first recall the effective description through an elastic line model before describing the implementation of Langevin molecular dynamics for this system. Section 4 presents a range of results, both for driven vortices in the steady state as well as for non-equilibrium relaxation processes that result from a quench of one of the external system control parameters. We conclude in section 5.

2. Langevin dynamics

Before we employ Langevin molecular dynamics for the investigation of the non-equilibrium properties of vortices in a disordered environment in the next section, it is useful to first illustrate the concept of a Langevin equation through simpler examples. For that reason we will briefly recall the case of a Brownian particle, followed by a general discussion of the Langevin equation of a system characterized by a Hamiltonian and the associated Boltzmann-Gibbs equilibrium probability distribution.

2.1. *Brownian particle*

The paradigmatic example of a Langevin equation is of course the stochastic equation that describes a particle immersed in a fluid. This particle is continuously exposed to collisions with the molecules of the fluid. Assuming that there is no net flow, the molecules hit the particle with the same rate from all sides, i.e., on average the force on the particle due to the fluid molecules is zero. In a probabilistic description this can be modeled by a stochastic force with zero mean. As the particle moves through the fluid, a hydrodynamic drag force sets in as a consequence of the random collisions with the fluid molecules that impedes the motion of the particle. Taking these two effects

into account, the equation of motion governing the particle is given by the Langevin equation

$$m \frac{d\mathbf{v}(t)}{dt} = -\eta \mathbf{v}(t) + \mathbf{f}(t) . \quad (1)$$

Here $\mathbf{v}(t)$ and m are the instantaneous velocity and the mass of the particle, respectively, η is the friction coefficient, and $\mathbf{f}(t)$ represents the stochastic force.

Before discussing the noise term further, let us stress that a stochastic description like equation (1) assumes a separation of time scales between slow degrees of freedom (in this case the particle) and fast degrees of freedom (the fluid molecules). Usually the fast degrees of freedom represent the environment in which the slow degrees evolve.

For the stochastic noise the following two assumptions are usually made: (1) the collisions of the fluid molecules with the particle are uncorrelated in time, and (2) the random forces are drawn from a Gaussian probability distribution with zero mean:

$$\langle \mathbf{f}(t) \rangle = 0 , \quad (2)$$

$$\langle f_\nu(t) f_\mu(t') \rangle = \gamma \delta_{\nu\mu} \delta(t - t') , \quad (3)$$

where ν and μ denote Cartesian coordinate indices and γ is the strength of the noise. While these assumptions are perfectly sound for a Brownian particle, one should make sure for each situation whether they are indeed meaningful for the problem at hand.

The noise term γ , which measures the strength of the fluctuations, and the friction coefficient η , which describes dissipation, are related through the fluctuation-dissipation theorem (called Einstein relation in the present context):

$$\gamma = 2k_B T \eta , \quad (4)$$

where T is the temperature of the environment and k_B is Boltzmann's constant.

If the inertia time is larger than m/η , inertial effects can be disregarded, and the particle's motion is then governed by the overdamped Langevin equation

$$\eta \frac{d\mathbf{r}(t)}{dt} = \mathbf{F}(\mathbf{r}(t)) + \mathbf{f}(t) , \quad (5)$$

where we have added a conservative force $\mathbf{F}(\mathbf{r}) = -\nabla V(\mathbf{r})$ originating from a potential $V(\mathbf{r})$. Equation (5) is in fact the starting point for Brownian dynamics as well as for Langevin molecular dynamics used in the following. Note that imposing the fluctuation-dissipation theorem ensures that this stochastic differential equation correctly describes the equilibrium properties of our particle.

2.2. Classical systems governed by a Hamiltonian

The overdamped Langevin equation (5) is readily generalized to situations with N degrees of freedom (spatial coordinates of the particles) governed by a Hamiltonian $H[\{\mathbf{r}\}]$ that is a functional of the position vectors \mathbf{r} of the different slow degrees of freedom. In that case one has the following set of coupled stochastic differential equations

$$\eta \frac{\partial \mathbf{r}_i(t)}{\partial t} = - \frac{\delta H[\mathbf{r}_i(t)]}{\delta \mathbf{r}_i(t)} + \mathbf{f}_i(t) , \quad (6)$$

where $i = 1, \dots, N$ labels the different particles. As before, the effects of the fast degrees of freedom coming from the environment are captured by the stochastic force $\mathbf{f}_i(t)$ acting on particle i . These

stochastic forces have again zero mean, $\langle \mathbf{f}_i(t) \rangle = 0$, and are taken from a Gaussian distribution, thereby fulfilling the Einstein relation (in d spatial dimensions)

$$\langle \mathbf{f}_i(t) \cdot \mathbf{f}_j(t') \rangle = 2d\eta k_B T \delta_{ij} \delta(t - t') . \quad (7)$$

This set of equations guarantees that in equilibrium the system samples configurations with the correct canonical equilibrium probability distribution, $\sim e^{-H/k_B T}$. However, out of equilibrium, which is our primary interest in the following, it is important to note that different microscopic dynamics might yield different results. This is even true in cases where the same probability distribution is ultimately obtained in equilibrium. A detailed comparison between different implementations of the system's dynamics might therefore be in order if one wishes to ascertain that out-of-equilibrium results are not merely artefacts of the dynamics (see, e.g., Ref. [6]).

3. Langevin molecular dynamics for interacting vortex matter

3.1. Elastic line model

We consider in the following N interacting elastic lines in a disordered environment. Having in mind magnetic flux lines in high- T_c superconductors, we remark that this situation corresponds to the extreme London limit with the superconducting coherence length much smaller than the London penetration depth [7]. Vortex lines are then described by their trajectories $\mathbf{r}_i(z)$, where z denotes the direction of the applied external magnetic field, and the two-dimensional vector \mathbf{r}_i indicates the xy position of line i at height z . As an immediate consequence of this description, magnetic flux lines in this model cannot form loops or overhangs, since $\mathbf{r}_i(z)$ has to be unique. This is a reasonable assumption, as long as the vortex energy per length (i.e., the elastic line tension) remains large compared to the energy scale of thermal fluctuations.

The effective Hamiltonian of this system is written as a functional of the vortex line trajectories with an extent of L in the z direction and consists of three competing terms: the elastic line energy, the external potential due to disordered pinning sites, and the repulsive vortex-vortex interaction:

$$\begin{aligned} H_N[\mathbf{r}_i] = & \frac{\tilde{\epsilon}_1}{2} \sum_{i=1}^N \int_0^L \left| \frac{d\mathbf{r}_i(z)}{dz} \right|^2 dz + \sum_{i=1}^N \int_0^L V_D(\mathbf{r}_i(z)) dz \\ & + \frac{1}{2} \sum_{i \neq j} \int_0^L V(|\mathbf{r}_i(z) - \mathbf{r}_j(z)|) dz . \end{aligned} \quad (8)$$

Consistent with the extreme London limit, the repulsive vortex-vortex pair interaction is set purely in-plane between different flux line elements. Below we will provide expressions for the attractive pinning potential and repulsive interaction appropriate for high- T_c superconductors.

In order to employ a Langevin molecular dynamics algorithm to simulate the vortex line dynamics, we discretize the system into layers along the z axis. Forces acting on the flux line vertices can then be derived from the properly discretized version of the Hamiltonian (8). We subsequently proceed to numerically solve the set of coupled overdamped Langevin equations

$$\eta \frac{\partial \mathbf{r}_i(t, z)}{\partial t} = - \frac{\delta H_N[\mathbf{r}_i(t, z)]}{\delta \mathbf{r}_i(t, z)} + \mathbf{f}_i(t, z) + \mathbf{F}_d . \quad (9)$$

As discussed in the previous section, the fast, microscopic degrees of freedom of the surrounding medium are captured by thermal stochastic forces $\mathbf{f}_i(t, z)$, modeled as uncorrelated Gaussian white noise with vanishing mean and fulfilling the Einstein relations (7) in $d = 2$ dimensions. This

guarantees that the system relaxes to thermal equilibrium with a canonical probability distribution in absence of an external driving force \mathbf{F}_d . In type-II superconductors such an external driving force stems from applied external currents via the Lorentz force.

The time integration is performed via simple discretization of equation (9) [8]. In Ref. [6] we also considered the situation of small inertia times. The Langevin equation then acquires an additional inertial term and the time stepping algorithm becomes slightly more complicated [9].

3.2. Implementation for disordered type-II superconductors

High- T_c superconducting materials are layered compounds and highly anisotropic: the lattice constant in the crystallographic c direction is much larger than the in-plane ones along the a and b directions; correspondingly, the effective charge carrier masses M_{ab} and M_c differ as well for the different directions. Henceforth we always assume that the magnetic field is aligned with the material's crystallographic c direction, and the material properties discussed below are given for this configuration and assigned the in-plane index ab . When discretizing the system into layers along the z axis we choose the crystallographic c axis unit cell size c_0 as layer spacing [10, 11].

This anisotropy also shows up in the expressions for the model parameters when using the effective elastic line model (8). The elastic line stiffness or local tilt modulus is given by $\tilde{\epsilon}_1 \approx \tilde{\Gamma}^{-2} \epsilon_0 \ln(\lambda_{ab}/\xi_{ab})$. Here λ_{ab} is the London penetration depth and ξ_{ab} is the coherence length, both in the ab plane, whereas $\tilde{\Gamma}^{-1} = M_{ab}/M_c$ denotes the effective mass ratio. The energy per length ϵ_0 is given by $\epsilon_0 = (\phi_0/4\pi\lambda_{ab})^2$, with the magnetic flux quantum $\phi_0 = hc/2e$. Finally the Bardeen-Stephen viscous drag coefficient η in the Langevin equation (9) is $\eta = \phi_0^2/2\pi\rho_n c^2 \xi_{ab}^2$, where ρ_n represents the normal-state resistivity [12].

For our implementation of the Langevin molecular dynamics method for disordered type-II superconductors [6, 13–15] we also require expressions for the vortex-vortex interaction as well as for the attractive pinning potential. The repulsive in-plane vortex-vortex interaction is given by

$$V(r) = 2\epsilon_0 K_0(r/\lambda_{ab}) , \quad (10)$$

where K_0 denotes the zeroth-order modified Bessel function. This is essentially a logarithmic repulsion that is exponentially screened at the scale λ_{ab} . In order to avoid artefacts due to periodic boundary conditions in directions perpendicular to z , we cut off the interaction at $5\lambda_{ab}$. Pinning sites are modeled by randomly distributed smooth potential wells of the form

$$V_\alpha(\mathbf{r}, t) = -\frac{b_0}{2} p \delta(z - z_\alpha) \left[1 - \tanh\left(5 \frac{|\mathbf{r} - \mathbf{r}_\alpha| - b_0}{b_0}\right) \right] , \quad (11)$$

where $p > 0$ is the pinning potential strength, and z_α and \mathbf{r}_α denote the z position and in-plane location of pinning site α , respectively. The pinning potential width b_0 will be our unit of length, whereas energies will be measured in units of $\epsilon_0 b_0$. The full pinning potential $V_D(\mathbf{r}, t)$ is then obtained by summing over all N_D localized pinning sites in the system:

$$V_D(\mathbf{r}, t) = \sum_{\alpha=1}^{N_D} V_\alpha(\mathbf{r}, t) . \quad (12)$$

For the case of random point defects, which is the only case considered in this paper, these pinning centers are randomly distributed and chosen independently for each layer. If one were to instead consider columnar defects aligned parallel to the magnetic field along the z direction, then one would repeat the same spatial distribution pattern for each layer [6, 14, 16].

The numbers we use for our model parameters are consistent with the actual values for YBCO [3]. We set the pinning potential width $b_0 = 35\text{\AA}$ and also choose $c_0 = b_0$. The superconducting coherence length is then given by $\xi_{ab} = 0.3 b_0$, whereas the London penetration depth is $\lambda_{ab} = 34 b_0$. The effective mass anisotropy ratio is $\tilde{\Gamma}^{-1} = 0.2$ and the normal-state resistivity near T_c becomes $\rho_n \approx 500 \mu\Omega \text{ cm}$. With this, the numerical values of all model parameters can be calculated. It then also follows that our fundamental temporal unit is $t_0 = \eta b_0 / \epsilon_0 \approx 18 \text{ ps}$. In the following we shall measure all time intervals in units of t_0 .

3.3. Quantities of interest

A large range of quantities of interest are at one's disposal when studying the out-of-equilibrium properties of vortex matter. Some of these quantities are especially useful to characterize the steady-state properties in the presence of an external driving force, others allow us to capture the complex relaxation processes in situations where the system is initialized far from a steady state.

A typical experimentally accessible quantity is the current-voltage (I-V) characteristics. From a Langevin molecular dynamics study an equivalent description is obtained from a graph relating the driving force \mathbf{F}_d to the mean vortex velocity \mathbf{v} . Indeed, from Faraday's law the mean vortex velocity, which results from the velocities of each line element in direction of the driving force, is related to an induced electric field $\mathbf{E} = \mathbf{B} \times \mathbf{v} / c$ and therefore to a voltage drop across the sample. A relation between the driving force \mathbf{F}_d and an applied external current density \mathbf{j} follows from the Lorentz force: $\mathbf{F}_d = \mathbf{j} \times \phi_0 \mathbf{B} / B$.

The thermal spatial fluctuations along the vortex lines can be captured by the radius of gyration. Defined as $r_g = \sqrt{\langle (\mathbf{r}_i(z) - \langle \mathbf{r}_i \rangle)^2 \rangle}$, this quantity is in fact nothing else than the average root mean-square displacement from the mean lateral positions of the lines. Here, $\langle \dots \rangle$ indicates an average over all line elements of line i as well as an average over all N lines and different realizations of the disorder and the noise.

A third way to explore steady-state properties of driven vortex matter is to study the pinning time statistics. This is done by calculating the distribution of flux line element dwelling times at defect sites. The dwelling time at pins is obtained by monitoring the positions of flux line elements and recording the instances where they enter and leave the attractive pinning centers.

Non-equilibrium relaxation processes are best studied by preparing a system in a specific state before suddenly changing a system parameter [5]. This sudden change, often referred to as a quench, can be realized in many ways, depending on the physical system under investigation. For disordered vortex matter the following three types of quenches can be realized experimentally: temperature quenches, magnetic field (or vortex density) quenches, and external current (i.e., driving force) quenches. After such a quench the system ends up in a state far from stationarity. The resulting relaxation processes can then be monitored through various quantities.

Many previous studies of glasses (structural glasses or spin glasses) as well as of systems with glassy-like dynamics have revealed that relaxation and related aging processes are best investigated through two-time quantities [5]. Indeed, as a system after the quench is far from stationarity, time translation invariance is broken and the properties of the system change with the time elapsed since the quench. As a result an observable that depends on two times s and $t > s$ is not only a function of the time difference $t - s$ but depends in more complicated ways on these two times.

In the context of interacting vortices in a disordered environment an impressive list of two-time quantities has been discussed [6, 14, 15, 17–21]. Some of these quantities contain information about local thermal fluctuations, whereas others provide insight into the time evolution of the global structure of the flux line configuration. We refrain from discussing all these quantities, but instead only introduce those used and displayed in the following concise overview: The height-height autocorrelation function (sometimes simply called the roughness) probes the local thermal

fluctuations of vortices about their mean lateral position. It is defined as

$$C(t, s) = \langle (\mathbf{r}_i(t, z) - \langle \mathbf{r}_i(t) \rangle) (\mathbf{r}_i(s, z) - \langle \mathbf{r}_i(s) \rangle) \rangle, \quad (13)$$

where the averages are again taken over the flux line elements of all lines as well as noise and disorder realizations. The average square distance between a vortex line element's position at the two times s and t is measured by the two-time mean square displacement

$$B(t, s) = \langle (\mathbf{r}_i(t, z) - \mathbf{r}_i(s, z))^2 \rangle. \quad (14)$$

This quantity contains information on the decay and formation of global structures.

4. Disordered vortex matter out of equilibrium

We illustrate the rich physics of interacting magnetic vortices in disordered type-II superconductors that is governed by competing energy and hence length and time scales, through various characteristic examples that address both fluctuations in non-equilibrium steady states [6, 13, 15] as well as complex out-of-equilibrium relaxation scenarios initiated from very different starting configurations [6, 14, 15]. In this brief overview, we focus on systems with comparatively weak magnetic fields and hence low vortex density, and at low temperatures. Consequently the equilibrium stationary configurations in the presence of attractive point-like pinning centers likely reside in the disorder-dominated Bragg glass thermodynamic phase, wherein spatial positional order is disrupted at long length scales. At the cost of elastic energy, the flux lines attempt to accommodate as many localized defect sites as possible, which renders their trajectories through the sample quite rough [22].

4.1. Driven vortex lines in disordered environments

When sufficiently large external currents are applied, the vortices detach from the pinning centers and freely flow through the sample. They then tend to reorder into regular triangular moving lattices. At zero temperature, the transition from the pinned, glassy phase with drift velocity $v = 0$ to the moving state with $v > 0$ is sharp, and represents a continuous non-equilibrium phase transition [23]. At finite temperatures, this transition becomes smoothed out as the external driving force F_d is increased. This is shown in Fig. 1 (top panel) for a Langevin molecular dynamics simulations of a system of $N = 16$ vortex lines (discretized into $L = 100 b_0$ layers transverse to the magnetic field) driven in a direction perpendicular to the external magnetic field, at temperature $T = 0.002 \epsilon_0 b_0 / k_B \approx 10$ K and with pinning strength $p = 0.05 \epsilon_0$. Below the depinning threshold $F_c \approx 0.002 \epsilon_0 / b_0$, the flux lines hardly move, but display thermal fluctuations; the system remains superconducting. For larger drives, the mean vortex speed scales linearly with the driving force. This indicates Ohmic dissipation, since $F_d \propto j$ and $v \propto E$, the induced electric field. Thus the freely flowing vortex system represents a normal-conducting phase.

The Langevin molecular dynamics simulations allow tracking of each individual vortex line, and hence a detailed analysis of the statistics of the transverse line fluctuations that are induced both thermally and through interactions with localized pinning sites. At large driving forces $F_d \gg F_c$, the attractions exerted by point defects become irrelevant, and thermal energies are also minute compared to the work associated with the drive. Consequently, the flux lines become straightened out, as is clearly seen in Fig. 1 (bottom panel), which displays the mean vortex radius of gyration as function of F_d . In the disorder-dominated Bragg glass phase, the gyration radius is enhanced by about a factor of three, indicating the roughness of the vortex trajectories. As F_d approaches F_c , the drive pulls more line segments away from the attractive defects, which increases the radius of

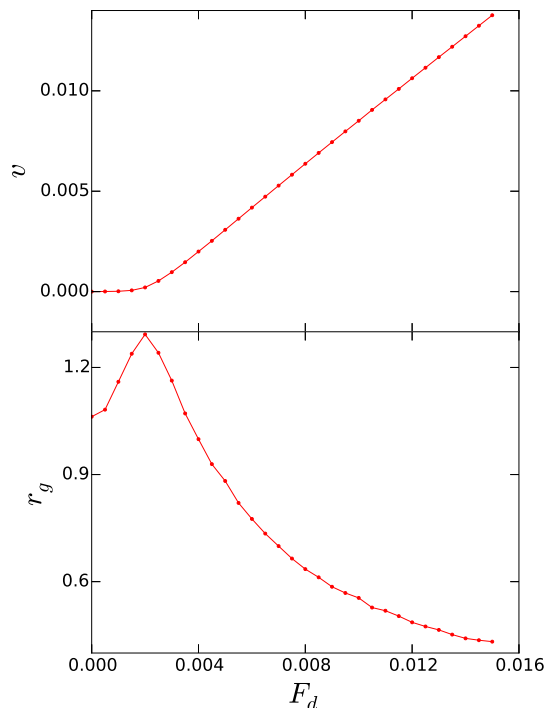


Figure 1. Mean vortex velocity v (top), in units b_0/t_0 , and flux line gyration radius r_g (bottom), in units of b_0 , in the non-equilibrium steady state vs. driving force F_d , in units of ϵ_0/b_0 , for a system of $N = 16$ interacting vortices of length $L = 100 b_0$ at temperature $T = 0.002 \epsilon_0 b_0/k_B$ and for point pinning center strength $p = 0.05 \epsilon_0$. The top graph directly maps onto the current-voltage characteristics for superconductors; the location of the gyration radius maximum in the bottom graph indicates the depinning threshold [15].

gyration. A distinct maximum of r_g is observed right at the depinning threshold, a clear signature of the aforementioned zero-temperature non-equilibrium phase transition, for which $r_g(F_d \rightarrow F_c) \rightarrow \infty$ would display a critical divergence [6, 15].

Even more detailed information on the pinning features of flux lines to variable point disorder is offered by careful analysis of the dwelling time statistics. Over many simulation runs, we recorded the durations τ that each line element of a single driven vortex (with $L/b_0 = 200$ segments) spent within a lateral distance b_0 of its previous position, and gathered the resulting histogram $P(\tau)$ [13]. We kept the driving force $F_d = 0.002 \epsilon_0/b_0$ fixed, but varied the temperature T and the width (standard deviation) w of an assumed Gaussian distribution for the pinning strengths p about the mean μ . Since the point defects are correlated only over a distance b_0 in our system, the collective Larkin-Ovchinnikov pinning length scale is $L_L \approx b_0(\tilde{\epsilon}_1/w)^{2/3}$. The associated typical energy barrier then becomes $E_L \approx \tilde{\epsilon}_1 b_0^2/L_L$, from which one estimates the critical depinning force as $F_c \approx E_L/(b_0 L_L) \approx w^{4/3}/(b_0 \tilde{\epsilon}_1^{1/3})$ [24]. Employing extreme-event statistics arguments, Vinokur, Marchetti, and Chen argued that in the pinned phase, the pinning time distribution should obey a power law for large dwelling times τ , $P(\tau) \sim \tau^{-1-\alpha(T)}$, with an effective temperature-dependent scaling exponent $\alpha(T) \sim k_B T/E_L$ [24].

This power-law behavior is indeed borne out by the Langevin molecular dynamics simulation data depicted in Fig. 2 (left panel, a) at large disorder variance $w = 1.0 \epsilon_0$. In contrast, in the weak pinning regime ($w = 0.001 \epsilon_0$), the vortices remain attached to the defects only for short times $\tau < 1000 t_0$, before they detach and freely flow through the system. The marked maximum of $P(\tau)$ observed in the corresponding graph may serve to define a typical pinning time $\tau \approx 700 t_0$. The dynamical phase diagram associated with the transition between the freely flowing and the pinned regime has been studied by Krauth et al by numerically extracting the structure factor exponent of an elastic string in the $T \rightarrow 0$ limit [25] and in the finite temperature case [26]. The right panel

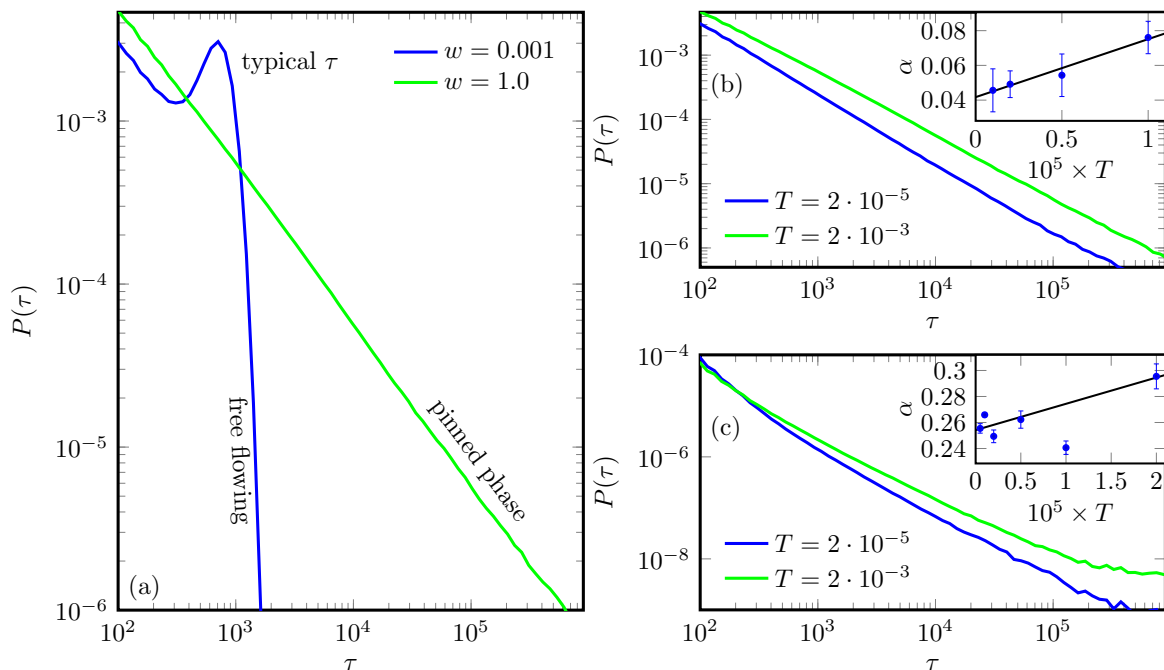


Figure 2. Left panel (a): Distribution of pinning times $P(\tau)$ for single vortices with $L/b_0 = 200$ line elements moving through a system with $N_D/L = 100$ randomly placed isolated point defects, whose pinning strengths are Gaussian distributed with mean $\mu = 0$ and variance w^2 ; driving force $F_d = 0.002 \epsilon_0/b_0$, temperature $T = 0.002 \epsilon_0 b_0/k_B$. In the flowing phase ($w = 0.001 \epsilon_0$), a characteristic dwell time can be extracted from the observed maximum. In the pinned phase ($w = 1.0 \epsilon_0$), $P(\tau)$ decays algebraically with τ . Right panel: (b) Temperature dependence of the power-law scaling and effective decay exponent $\alpha(T)$ for the pinning time distribution $P(\tau)$ (with T measured in units of $\epsilon_0 b_0/k_B$). (c) Similar results, but obtained for a continuous Gaussian disorder landscape correlated over distance $\xi = b_0$ with otherwise identical parameter values [13].

(b) of the figure explores the temperature dependence of the effective decay exponent $\alpha(T)$; as the inset for the low-temperature regime $T \leq 10^{-5} \epsilon_0 b_0/k_B$ confirms, one indeed finds a roughly linear dependence $\alpha(T) \approx 0.0417 + 3340 T$, albeit with an apparent non-zero intercept as $T \rightarrow 0$ [13] that is not captured by the scaling theory. We also investigated the dwelling time distribution where the discrete point defects are replaced by a smooth, continuous disorder landscape, in order to make more direct contact with the theoretical setting in Ref. [24]. To this end, we drew the pinning potential strength p at each node of a square lattice with spacing b_0 from a Gaussian distribution with vanishing mean at variance w^2 , and constructed the continuous landscape from the resulting grid points through straightforward bi-linear interpolation. In the pinned state, one again observes algebraic decay of $P(\tau)$, but actually less cleanly, as shown in the the right panel (c) of Fig. 2; also, the typical dwelling time in this situation turns out to be $\tau \approx 100 t_0$, indicating a different overall energy scale as compared with the discrete pin case. At low temperatures, we found the linear relationship $\alpha(T) \approx 0.2542 + 2019 T$ (inset) [13].

4.2. Relaxation dynamics of vortex lines in disordered type-II superconductors

Next we proceed to investigate the non-equilibrium relaxation kinetics of vortex matter in disordered type-II superconductors starting from various initial configurations that are quite distinct from the stationary states that may be reached after long time durations. In this brief overview, we report Langevin molecular dynamics simulation data for mutually interacting flux lines subject to randomly distributed attractive point pinning centers, and probe the relaxation kinetics through the various two-time quantities introduced in section 3.3. We first study simulations for systems where initially perfectly straight vortex lines were placed at random positions in the sample, and then allowed to relax towards Bragg glass equilibrium states at low temperatures

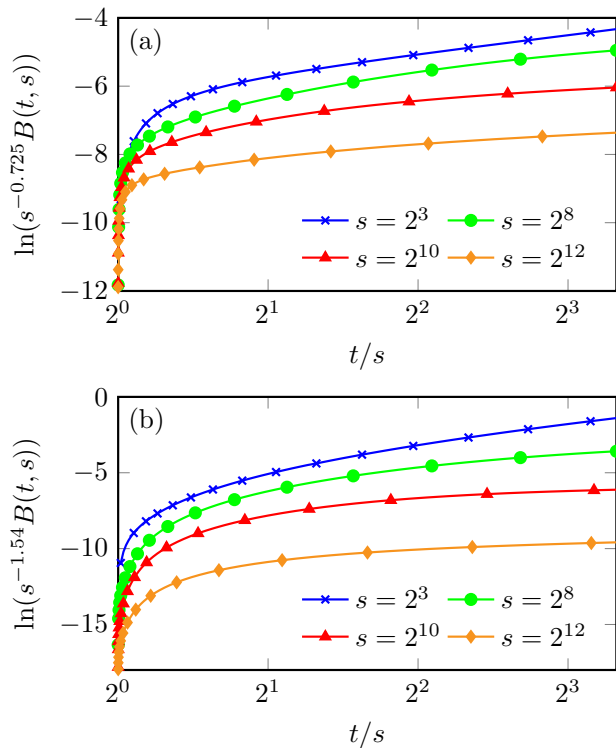


Figure 3. Relaxation of the two-time mean-square displacement $B(t, s)$ for flux lines of length $L = 640 b_0$ subject to attractive point defects of strength $p = 0.05 \epsilon_0$, at temperature $T = 0.002 \epsilon_0 b_0 / k_B$, and for various waiting times s as indicated, starting from initially straight vortices placed at random locations: (a) in the absence of mutual interactions; (b) in the presence of repulsive forces. Simple aging scaling collapse of the data can only be achieved for small waiting times s , with the aging exponents $b \approx 0.725$ and $b \approx 1.54$. [6].

$T = 0.002 \epsilon_0 b_0 / k_B \approx 10\text{K}$ at vanishing driving force $F_d = 0$. We shall attempt to fit the data to the simple aging scaling form $A(t, s) \sim s^b F_A(t/s)$ for two-time observable A with the aging exponent b . Indeed, in the absence of disorder and mutual vortex interactions, this setup leads to simple aging scaling for both the two-time mean-square displacement $B(t, s)$ and the two-time height-height autocorrelation function $C(t, s)$ with the Edwards-Wilkinson scaling exponent $b = 0.5$ [6, 19, 27].

In the presence of attractive point-like pinning centers, however, such simple aging scaling behavior is not observed, although time translation invariance is manifestly broken. Figure 3 displays data for the two-time mean-square displacement for various waiting times s , both for non-interacting flux lines (a) and mutually repelling vortices (b) with $L/b_0 = 640$ segments. Simple aging data collapse can only be obtained at short times s , with the scaling exponents $b \approx 0.725$ and $b \approx 1.54$, respectively. Non-interacting vortices strive to optimize the balance between pinning energy gains and elastic stretching energy losses. Interacting flux lines in addition become ‘caged’ through the repulsive interactions with their neighbors, which drastically reduces lateral line fluctuations and displacements. These same competitive effects are visible also in the simulation data for the height-height autocorrelation function $C(t, s)$. Simple aging scaling again ensues only for very short waiting times s , with, e.g., a scaling exponent $b \approx 0.716$ for non-interacting vortices as indicated in Fig. 4(a). The competition between elastic forces and pinning induce remarkably complex and even non-monotonic relaxation features. When the repulsive in-plane pair interactions between flux line elements are taken into account, the two-time height-height autocorrelation data display characteristic two-step relaxation behavior, see Fig. 4(b), as is also frequently seen in structural and spin glasses [28]. In the ‘ β ’ relaxation time window, $C(t, s)$ changes hardly at all, and the data appear to satisfy time translation invariance; in the ultimate ‘ α ’ relaxation regime, the normalized height-height autocorrelation function finally decays, albeit very slowly [6].

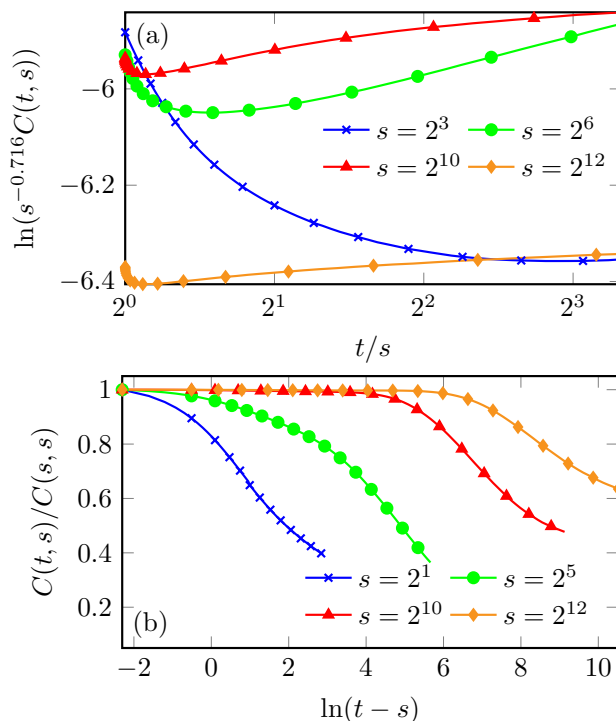


Figure 4. Relaxation of the two-time height-height autocorrelation function $C(t, s)$ for flux lines of length $L = 640 b_0$ subject to attractive point defects of strength $p = 0.05 \epsilon_0$, at temperature $T = 0.002 \epsilon_0 b_0 / k_B$, and for various waiting times s as indicated, starting from initially straight vortices placed at random locations: (a) in the absence of mutual interactions; (b) in the presence of repulsive forces. [6].

We pause for a moment to mention the work of Bustingorry et al [17, 18] in which relaxation processes in a related system were studied using Langevin molecular dynamics. In that work both attractive and repulsive pinning sites were present in the system. This modification yields important changes in the relaxation processes. For instance, instead of observing the two-step glassy-like relaxation shown in Fig. 4, a simple aging scaling of the autocorrelation prevails.

Experimentally, the initial configuration of randomly placed straight vortices studied above cannot be realized. In order to address more realistic initial conditions, we therefore ran a series of numerical experiments wherein the system is allowed to relax for 10^5 time steps, until at $t = 100,000 t_0$ a sudden change of an external experimental control parameter is implemented. We then monitored several observables to characterize the system's non-equilibrium relaxation features following such quenches. A first example is depicted in Fig. 5: At the quench point, the system's temperature was instantaneously raised from $T = 0.002 \epsilon_0 b_0 / k_B$ to $T = 0.008 \epsilon_0 b_0 / k_B$. Both the radius of gyration $r_g(t)$ and the fraction of pinned flux line elements $\varphi(t)$, defined as the fraction of segments that reside within a distance b_0 of the attractive point pins at time t , are seen to relax essentially exponentially towards the system's new steady state at elevated temperature. For the gyration radius, the relaxation time in Fig. 5(a) is measured to be $\tau \approx 34600 t_0$. Asymptotically, the temporal evolution approaches that of an unperturbed vortex sample at the higher temperature. Careful inspection of Fig. 5(a) reveals a tiny dip immediately following the quench before the expected larger gyration radius value at elevated temperature is reached. Indeed, as confirmed in panel (b), at first a few line elements become thermally depinned by the sudden temperature increase, which initially slightly relaxes the disorder-induced vortex line roughening in the Bragg glass phase. At any rate, the exponentially fast relaxation prevents the emergence of a sizeable aging time window [14].

Considerably richer and more complex relaxation features are observed following a magnetic field quench at time $r = 100,000 t_0$, when the number of vortices in the system is either suddenly

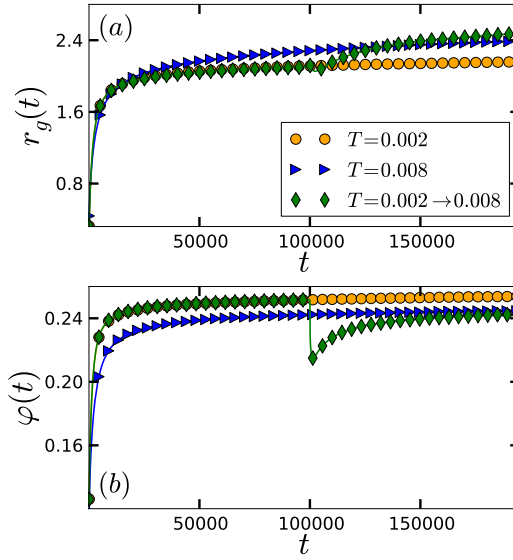


Figure 5. Time evolution of (a) the radius of gyration $r_g(t)$, and (b) the fraction of pinned vortex line elements $\varphi(t)$, following a sudden temperature quench from $T = 0.002 \epsilon_0 b_0 / k_B$ to $T = 0.008 \epsilon_0 b_0 / k_B$ at $t = 100,000 t_0$ for a system of $N = 16$ interacting flux lines of length $L = 640 b_0$ subject to attractive point defects of strength $p = 0.05 \epsilon_0$. For comparison, the time tracks at fixed initial and final temperatures are shown as well. The system relaxes exponentially fast to its new steady state [14].

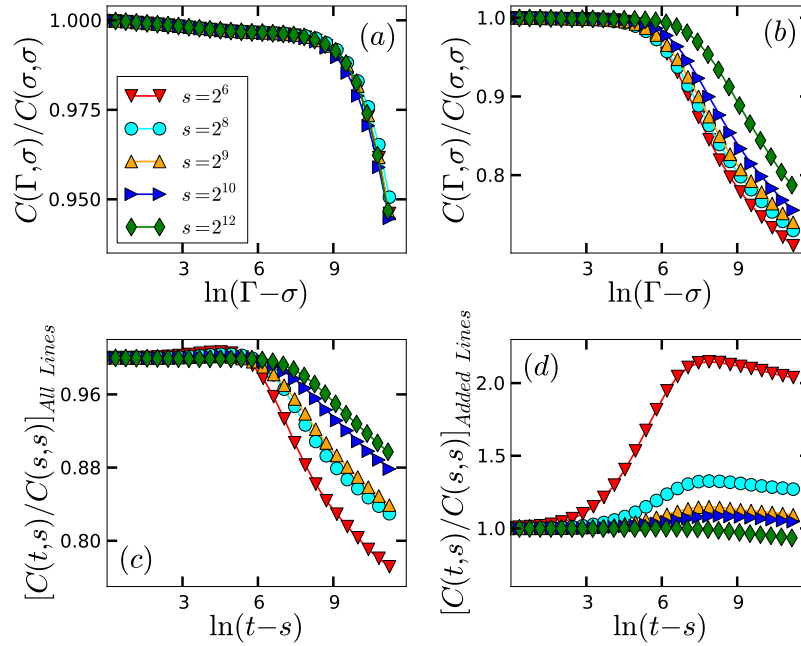


Figure 6. Relaxation of the normalized two-time height-height autocorrelation function for various waiting times s (as indicated) at temperature $T = 0.002 \epsilon_0 b_0 / k_B$ for flux lines of length $L = 640 b_0$ subject to attractive point defects of strength $p = 0.05 \epsilon_0$ (a) at fixed magnetic field or flux density, with $N = 16$ flux lines in our simulation sample; (b) following a field down quench, suddenly reducing the vortex number from $N = 21$ to 16; (c) following a field up quench, where 5 additional flux lines are added to the original $N = 16$ vortices; (d) as in (c), but displaying the data only for the 5 newly added flux lines [14].

reduced (down quench) or increased (up quench), in both cases maintaining a fixed temperature $T = 0.002 \epsilon_0 b_0 / k_B$ (and a vanishing driving force $F_d = 0$). We introduce the total elapsed simulation times $\Gamma = r + t$ and $\sigma = r + s$; since r will be much larger than the times s and t , both measured after the quench at r , the shift by the duration r needs to be taken into account in attempts to achieve simple aging scaling. Figure 6(a) displays the relaxation curves for the normalized two-time

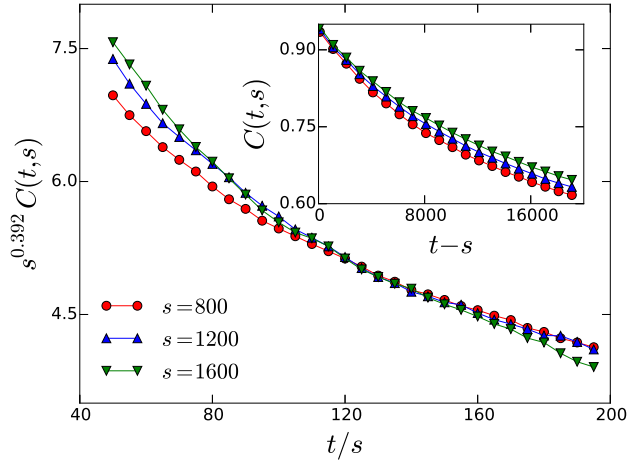


Figure 7. Time evolution of the two-time height-height autocorrelation function for various waiting times s (as indicated) at temperature $T = 0.002 \epsilon_0 b_0 / k_B$ for driven flux lines of length $L = 640 b_0$ subject to attractive point defects of strength $p = 0.05 \epsilon_0$, as the driving force is instantaneously reduced from $F_d = 0.015 \epsilon_0 / b_0$ (i.e., from a moving non-equilibrium steady state) into the pinned Bragg glass phase at $F_d = 0.001 \epsilon_0 / b_0$. The inset shows the data plotted vs. $t - s$, demonstrating the breaking of time translation invariance; the main panel indicates the best attempt to fit the data to a simple aging scaling form with $b = 0.392$, which however only partially works in a very limited time window [15].

height-height autocorrelation function with the magnetic field or vortex density held constant for various waiting times $s = \sigma - r$; the data essentially correspond to the longest waiting time curve in Fig. 4(b) and demonstrate that for the large duration $r = 10^5 t_0$ considered here, the vortex system has basically reached the stationary regime for which time translation invariance holds: the data collapse when plotted against the time difference $\Gamma - \sigma = t - s$. In contrast, clear evidence of broken time translation invariance is visible in Fig. 6(b), where at $r = 100,000 t_0$ five randomly selected vortices were instantaneously removed from the system. One still observes the α - β two-step relaxation scenario, yet the system has not reached stationarity yet, akin to Fig. 4(b) [14].

Qualitatively very similar relaxation features are observed in the system of originally $N = 16$ vortices, when at $r = 100,000 t_0$ five new and initially straight flux lines are introduced at random positions in the sample, as seen in Fig. 6(c). Time translation invariance is again manifestly broken in the late α relaxation regime. By separately assessing the relaxation data for the two-time height-height autocorrelation function of just the newly added flux lines, depicted in Fig. 6(d), it becomes apparent that the distinction between Figs. 6(b) and (c) are caused by the marked non-monotonic behavior of the lateral line fluctuation relaxations of the added line population, which typically first show a strong increase followed by a much slower final decay. Only at very long waiting times $s \geq 2^{12} t_0$ do we observe the monotonic α - β relaxation features. When the new vortices are inserted into the sample, they experience strong repulsive forces from the originally present flux lines, which increases their range and thus facilitates their pinning to point defects. This in turn enhances transverse line fluctuations, until at $\ln(t - s) \approx 7$ optimal pinning configurations have been reached, whence the final slow decay of the autocorrelation function ensues [14].

As a final set of numerical experiments, we initialize the vortex system with $N = 16$ lines at temperature $T = 0.002 \epsilon_0 b_0 / k_B$ and at sufficiently large external driving force $F_d = 0.015 \epsilon_0 / b_0$ to ensure it resides well in the moving non-equilibrium steady state, see Fig. 1. After relaxing the system for a duration of $200,000 t_0$, the drive is suddenly lowered to $F_d = 0.001 \epsilon_0 / b_0$, which forces the flux lines into the pinned, disorder-dominated Bragg glass phase. Subsequently, we again monitor various observables; as characteristic example, the relaxation data for the two-time height-height autocorrelation function $C(t, s)$ are shown in Fig. 7. As in the previous magnetic field quench scenarios and for randomized initial conditions, simple aging scaling does not ensue for this quantity, but holds only approximately in a very limited time regime (with scaling exponent $b \approx 0.392$). It is worth mentioning that upon starting in the pinned glassy state, and suddenly increasing the

driving force into the moving state, the relaxation processes occur exponentially fast and quickly reach stationarity, with relaxation times of the order of $1200 t_0$ [15].

5. Conclusion

Langevin molecular dynamics is a powerful numerical method for the investigation of interacting systems with many degrees of freedom and clear separation of time scales. In this paper we have illustrated this through the study of interacting vortex matter in different far-from-equilibrium situations. We focused on values for the system parameters that are realistic for high- T_c superconductors. When driving the vortices through the sample by means of an external current, non-equilibrium steady states and a (zero temperature) non-equilibrium phase transition emerge. As the Langevin molecular dynamics simulations allow to track each individual vortex line, a detailed investigation of the steady-state properties is possible through the measurement of a variety of quantities. A second experimentally relevant situation arises when a system is brought out of equilibrium through a rapid change (quench) of some of the external system control parameters. Vortex matter in a disordered environment provides an extremely rich and technologically important model system, with a variety of such perturbations that are experimentally feasible, namely temperature, magnetic field, as well as current quenches. Detailed investigations of these different situations allow us to gain a rather complete understanding of the relaxation processes that take place when interacting vortex matter is forced out of thermal equilibrium.

Funding

This research is supported by the U.S. Department of Energy, Office of Basic Energy Sciences, Division of Materials Sciences and Engineering under Award DE-FG02-09ER46613.

References

- [1] Ciffey WT, Kalmykov YP. *The Langevin Equation: With Applications to Stochastic Problems in Physics, Chemistry and Electrical Engineering*. 3rd ed. Singapore: World Scientific Publishing; 2012.
- [2] Langevin P. Sur la théorie du mouvement brownien. *C. R. Acad. Sci. (Paris)* 1998;146:530–533.
- [3] Blatter G, Geshkenbein VB, Larkin AI, Vinokur VM. Vortices in high-temperature superconductors. *Rev. Mod. Phys.* 1994;66:1125–1388
- [4] Struik LCE. *Physical aging in amorphous polymers and other materials*. Amsterdam: Elsevier; 1978.
- [5] Henkel M, Pleimling M. *Nonequilibrium phase transitions Volume 2 – Ageing and Dynamical Scaling far from Equilibrium*. Heidelberg: Springer; 2010.
- [6] Dobramysl U, Assi H, Pleimling M, Täuber UC. Relaxation dynamics in type-II superconductors with point-like and correlated disorder. *Eur. Phys. J. B* 2013;86:228.
- [7] Nelson DR, Vinokur VM. Boson localization and correlated pinning of superconducting vortex arrays. *Phys. Rev. B* 1993;48:13060–13097.
- [8] Brass A, Jensen HJ. Algorithm for computer simulations of flux-lattice melting in type-II superconductors. *Phys. Rev. B* 1989;39:9587–9590.
- [9] Brünger A, Brooks CL, Karplus M. Stochastic boundary conditions for molecular dynamics simulations of ST2 water. *Chem. Phys. Lett.* 1984;105:495–500.
- [10] Das J, Bullard TJ, Täuber UC. Vortex transport and voltage noise in disordered superconductors. *Physica A* 2003;318:48–54.
- [11] Bullard TJ, Das J, Daquila GL, Täuber UC. Vortex washboard voltage noise in type-II superconductors. *Eur. Phys. J. B* 2008;65:469–484.
- [12] Bardeen J, Stephen M. Theory of the motion of vortices in superconductors. *Phys. Rev. A* 1965;140:1197–1207.

- [13] Dobramysl U, Pleimling M, Täuber UC. Pinning time statistics for vortex lines in disordered environments. *Phys. Rev. E* 2014;90:062108.
- [14] Assi H, Chaturvedi H, Dobramysl U, Pleimling M, Täuber UC. Relaxation dynamics of vortex lines in disordered type-II superconductors following magnetic field and temperature quenches. arXiv:1505.06240 2015.
- [15] Chaturvedi H, Assi H, Dobramysl U, Pleimling M, Täuber UC. Vortex dynamics in type-II superconductors following current quenches. In preparation 2015.
- [16] Pleimling M, Täuber UC. Characterization of relaxation processes in interacting vortex matter through a time-dependent correlation length. arXiv:1507.07283 2015.
- [17] Bustingorry S, Cugliandolo LF, Domínguez D. Out-of-equilibrium dynamics of the vortex glass in superconductor. *Phys. Rev. Lett.* 2006;96:027001.
- [18] Bustingorry S, Cugliandolo L F, Domínguez D. Langevin dynamics of the out-of-equilibrium dynamics of the vortex glass in high-temperature superconductor. *Phys. Rev. B* 2007;75:024506.
- [19] Bustingorry S, Cugliandolo LF, Iguain JL. Out-of-equilibrium relaxation of the Edwards-Wilkinson elastic line. *J. Stat. Mech.* 2007:P09008.
- [20] Iguain JL, Bustingorry S, Kolton AB, Cugliandolo LF. Growing correlations and aging of an elastic line in a random potential. *Phys. Rev. B* 2009;80:094201.
- [21] Pleimling M, Täuber UC. Relaxation and glassy dynamics in disordered type-II superconductors. *Phys. Rev. B* 2011;84:174509.
- [22] Nattermann T, Scheidl, S. Vortex-glass phases in type-II superconductors. *Adv. Phys.* 2000;49:607–704.
- [23] Fisher DS, Fisher MPA, Huse DA. Thermal fluctuations, quenched disorder, phase transitions, and transport in type-II superconductors. *Phys. Rev. B* 1991;43:130–159.
- [24] Vinokur VM, Marchetti MC, Chen L-W, Glassy motion of elastic manifolds. *Phys. Rev. Lett.* 1996;77:1845–1849.
- [25] Kolton AB, Rosso A, Giamarchi T, Krauth W, Dynamics below the depinning threshold in disordered elastic systems. *Phys. Rev. Lett.* 2006;97:057001.
- [26] Kolton AB, Rosso A, Giamarchi T, Krauth W, Creep dynamics of elastic manifolds via exact transition pathways. *Phys. Rev. E* 2009;79:184207.
- [27] Röthlein A, Baumann F, Pleimling, M. Symmetry based determination of space-time functions in nonequilibrium growth processes. *Phys. Rev. E* 2006;74:061604.
- [28] Götze W, Sjogren L. Relaxation processes in supercooled liquids. *Rep. Prog. Phys.* 1992;55, 241–376.